COMPARATIVE ANALYSIS OF BEARING HEALTH MONITORING METHODS FOR MACHINE TOOL LINEAR AXES

N. Jordan Jameson and Gregory W. Vogl
Engineering Laboratory
National Institute of Standards and Technology (NIST)
100 Bureau Drive
Gaithersburg, MD 20899
Telephone: (301) 975-8966
noel.jameson@nist.gov

Abstract: The study of rotating machinery ball bearing diagnostics and prognostics is quite mature and an abundance of methods/algorithms are available to perform these functions. However, extending these algorithms to other ball bearing applications is challenging and may not yield usable results. This work used a linear axis testbed to study the ability of an inertial measurement unit to measure changes in geometric error motions. Faults were introduced on the recirculating ball bearings of one carriage truck with increasing severity. The inertial measurement unit data was analyzed using a variety of methods proposed and used in the rotating machinery community, including auto-regressive filtering, minimum entropy deconvolution, and spectral kurtosis. The results reveal an ineffectiveness of the methods for the induced faults, for this one experiment, which have low signal-to-noise ratio and/or weaker periodicity than faults in rotating machinery.

Keywords: Linear axis, ball bearing, degradation, diagnostics, smart manufacturing

Introduction: Linear translational axes are important systems in manufacturing, often installed as a subsystem of a computer numerical control (CNC) machine. They are used to move cutting tools and workpieces to their desired positions for part production [1]. In a typical machine, there can be multiple such axes, each of which can degrade, producing inaccuracies that affect the quality of the parts produced. A single linear axis is shown in Figure 1(a), with each of the main components labeled. Four trucks (also called “linear motion guides”) are used to guide the carriage along the axis rails using recirculating ball bearings.

As a linear axis operates over time, abrasion and adhesion between parts causes material fatigue, pitting, cracking, and wear. This can result in faults developing in a variety of components such as the axis rails, rolling element bearings, and/or ball screw [2, 3]. If not properly mitigated, these faults will develop to such an extent as to affect the quality of the parts produced and/or precipitate a failure of the machine [4]. As demands for versatility and batch volume increase for manufacturing processes, machines are experiencing higher loads, and as a result the potential for faults and failures are becoming more common.

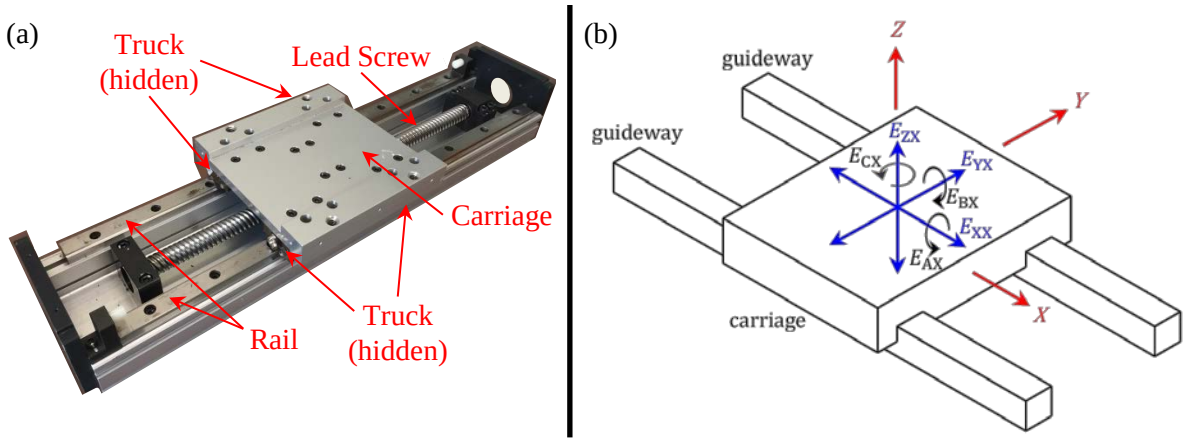

Figure 1: (a) Linear axis. The carriage travels along the axis of the lead screw and four trucks guide the carriage along the two rails (or guideways). (b) Angular and linear error motions of a carriage commanded to move along a (nominal) straight-line trajectory parallel to the X-axis.

The health assessment process consists of measuring the error motions of the linear axis machine and comparing those with specifications for allowable errors. In a linear axis, there are six degrees of freedom corresponding to six error directions, as shown in Figure 1(b), where the second variable in the subscript denotes the direction of travel (in this case, the carriage is traveling in the X-direction). In the schematic, E_{XX} denotes the linear positioning error motion of the X-axis, E_{YX} denotes the straightness error motion in the Y-direction, E_{ZX} denotes the straightness error motion in the Z-direction, E_{AX} denotes the angular error motion around the X-axis (roll), E_{BX} denotes the angular error motion around the Y-axis (pitch), and E_{CX} denotes the angular error motion around the Z-axis (yaw).

Ideally, after a linear axis is installed on a machine tool, all errors are zero, but in practice nonzero errors exist resulting in the errors on the workpiece. Hence, the allowable errors are dependent upon the tolerance needed for the workpiece. As the machine ages or crashes occur as a result of programming mistakes, these errors can increase leading to the workpieces becoming more and more out of tolerance. Instructive machine tool monitoring coupled with proper maintenance regimes can be used to mitigate this accumulation of degradation and minimize the costs imposed by imperfect production and scrapped parts.

Mature methods for the fault detection and diagnostics of linear axes are manual, time consuming, and often cost prohibitive. The state-of-the-art instruments in linear axis error measurement (the basis for diagnostics) are explained in ISO 230-1 [5]: straightedge and linear displacement sensor, microscope and taut wire, alignment telescope, alignment laser, and laser straightness interferometer. These time-consuming instruments require the shutdown of the machine and thus cannot provide in-situ diagnostics [6].

To ease the burden of implementing the traditional monitoring technologies, manufacturers need automated and efficient methods for diagnosing machine tool linear axes without halting production. In 2010, Teti *et al.* [7] identified that new sensors and sensor systems, advanced sensor signal data processing, and intelligent sensor monitoring need to be further developed

to help achieve decreased machine downtime, higher productivity, higher product quality, and enhanced knowledge of manufacturing processes.

Previous work has shown that a possible advance in sensor technology lies in the use of an inertial measurement unit (IMU) consisting of a 3 degree-of-freedom (DOF) accelerometer and a 3 DOF rate gyroscope [8-10] as shown in Figure 2. The bandwidths and noise properties of the sensors used in the IMU are shown in Table 1. Data from the IMU can be used to detect changes in the positioning, straightness, and angular error motions. IMU measurements can be made quickly and with little intrusion into the operation of the machine, resulting in data that provides insight into the condition of the linear axis. It has been shown to be effective at detecting rail degradation to similar levels of accuracy delivered by a laser interferometer [8]. However, a challenge remains in verifying the IMU's capabilities for detecting degradation in the truck bearings of a linear axis.

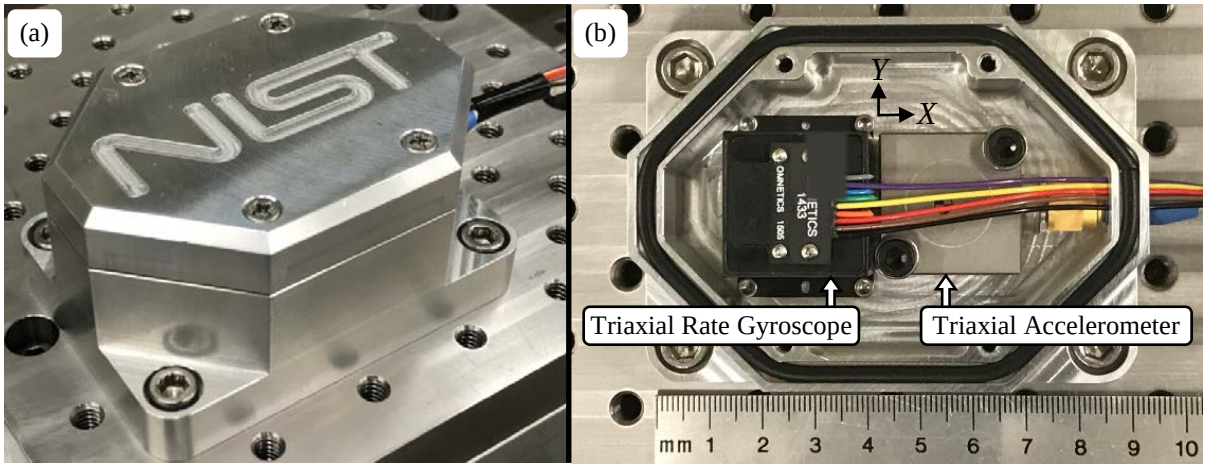

Figure 2: (a) Isometric view of industrial IMU and (b) top view of industrial IMU without its cover.

Table 1: Specified properties of sensors used in the IMU

Sensor	Bandwidth*	Noise
Accelerometer	0 to 400 Hz	$69\ (\mu m/s^2)/\sqrt{Hz}$
Rate Gyroscope	0 to 200 Hz	$35\ (\mu rad/s^2)/\sqrt{Hz}$

*frequencies correspond to half-power points, also known as 3 dB points

One complication that presents itself in this task is the multiplicity in the rolling element bearings within the bearing system, which causes a low signal-to-noise ratio (that can be less than 1) in the health monitoring data. In the linear axis shown in Figure 1(a), there are four trucks, each with two loops of ball bearings, and each loop has 32 ball bearings. The ball bearings rotate in and out of contact with the rail, with about 13 ball bearings per loop contacting the rail at any given instance. The two loops interact with different raceways (or grooves) in the rails, one inner and one outer. Hence, at any given instance, there are about 104 bearings (13 bearings per loop × 2 loops per truck × 4 trucks) in contact with the rails. The convolution of so many bearing ball signatures into the sensed effects on the carriage make it

difficult to isolate small indications of damage from a single bearing ball. This interaction between the bearings and rails is illustrated in Figure 3(a) and Figure 3(b). It was with this in mind that an experiment was designed to examine the sensitivity of the IMU-based error motions to artificially-induced damage on the bearings.

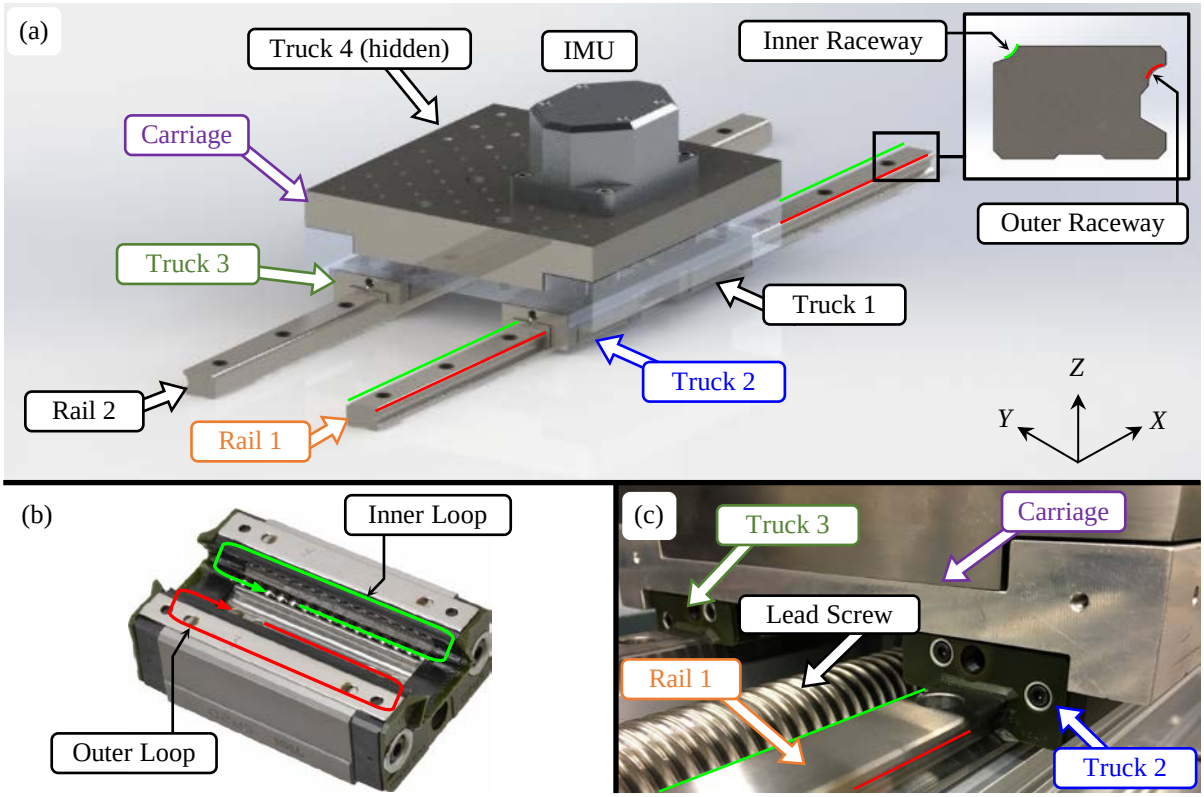

Figure 3: (a) Schematic of rails and carriage assembly of one-axis testbed; (b) underside view of one truck with loops of ball bearings exposed, where the “inner loop” contacts the inner raceway and the “outer loop” contacts the outer raceway; and (c) view of rail, carriage, lead screw, and trucks assembly showing the attachment of the trucks to the rails.

In this study, ball bearings from a single truck were removed sequentially, one-at-a-time, intentionally degraded, then replaced in their original position within the truck. The balls were degraded one at a time to progressively alter the error motions of the carriage. IMU data was collected after each ball bearing was damaged and the data was analyzed to develop diagnostic features. The data analysis procedure progressed from less to more complex culminating in a series of algorithms recommended by Randall and Antoni in their 2011 bearing diagnostics tutorial [11].

Experimental Setup: Truck 2 was modified to allow the removal of one ball at a time. This permitted the opportunity to inflict damage on to a single ball and then replace it into the truck, while leaving the carriage/truck/rail/lead screw system effectively unchanged. This was necessary because if the trucks were removed and then reassembled at each stage of degradation, then the load placed upon each of the trucks would have changed from one assembly procedure to the next, which would have changed the error motions as well. Hence, to eliminate the need for disassembly and reassembly of the trucks during the experiment and

thus ensure that changes in error motions are due only to bearing ball damage in truck 2, the truck was modified with an access hole and slot, as shown in Figure 4(a). The set screw covered the access hole from which balls were removed to introduce damage. Bearing balls were removed one-at-a-time and a "flat" was introduced by dragging the ball across sandpaper. The flat damage for one bearing is shown in Figure 4(b). After damaging the bearing, it was replaced in Truck 2 at its original position within the outer ring.

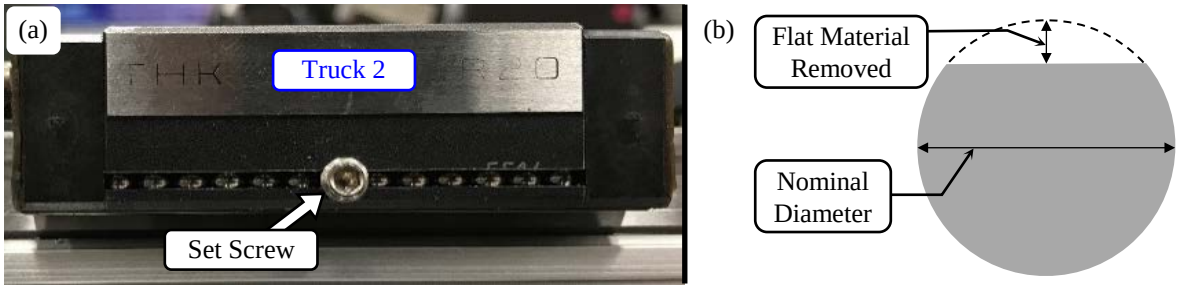

Figure 4: (a) Truck 2 as modified for this experiment with a slot for viewing the bearing movement and an access hole covered by a set screw, which allowed for the removal of single bearing ball; and (b) diagram showing the damage introduced to the balls in Truck 2.

Over the course of the experiment, 26 of the 32 bearing balls in the outer loop of Truck 2 were damaged. Figure 5 shows the pattern of twenty-six metal balls with six (black) silicon nitride balls. The pattern was chosen so that at any time, visual inspection of the balls through the slot, as seen in Figure 4(a), yields a unique pattern of black and silver (metallic) balls for identification. The twenty-six metal balls were made of chromium steel with a nominal diameter of 3.962 mm $\pm$ 0.001 mm, while the six ceramic balls had a nominal diameter of 3.969 mm $\pm$ 0.0008 mm. The average depth of material removed for the chromium steel balls was 30 µm with a standard deviation of 2 µm. The maximum depth was 35 µm and the minimum depth was 26 µm. The Truck 2 outer loop balls were degraded in a specific order, as shown in Figure 5, that attempts to increase general frequency content of defect-induced impulses.

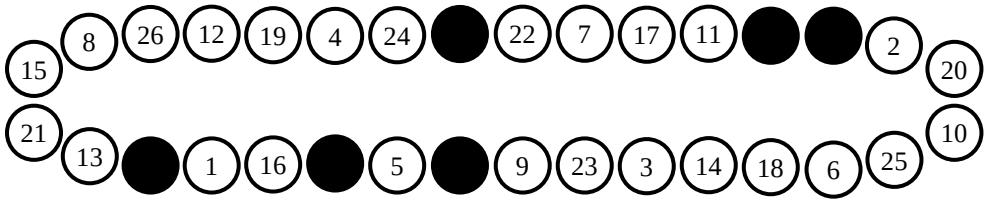

Figure 5: Truck 2 outer loop bearing degradation arrangement. The filled in circles represent ceramic bearing balls that were not degraded, while the numbers in the open circles denote the order in which the remaining metal balls were damaged.

After a single bearing was degraded and placed back into Truck 2, 50 runs of IMU data was gathered and processed to yield the estimated error motions for the carriage. Each run consists of moving the carriage over the linear axis, forward and backward, at three different speeds: 0.02 m/s, 0.1 m/s, and 0.5 m/s. These three speeds are meant to capture different ranges in the spatial frequency spectrum, with the slowest speed capturing the highest spatial frequencies

and the highest speed capturing the lowest spatial frequencies. With the rate gyroscope and accelerometer used, the available spatial frequency range is between 0 and 2 cycles/mm (this can also be written as 2000 m^{-1}). (For more information on how the rate gyroscope and accelerometer data was processed to achieve the error motion data, see [8, 9].) Hence, for each of 27 degradation "stages", there are fifty (50) data runs to be analyzed. Stage 1 is collected prior to any balls being degraded, and data collection ended at stage 27 with 26 of the balls having been damaged. The first sample for stages 1, 9, 18, and 27 are shown in Figure 6 for all six degrees of freedom.

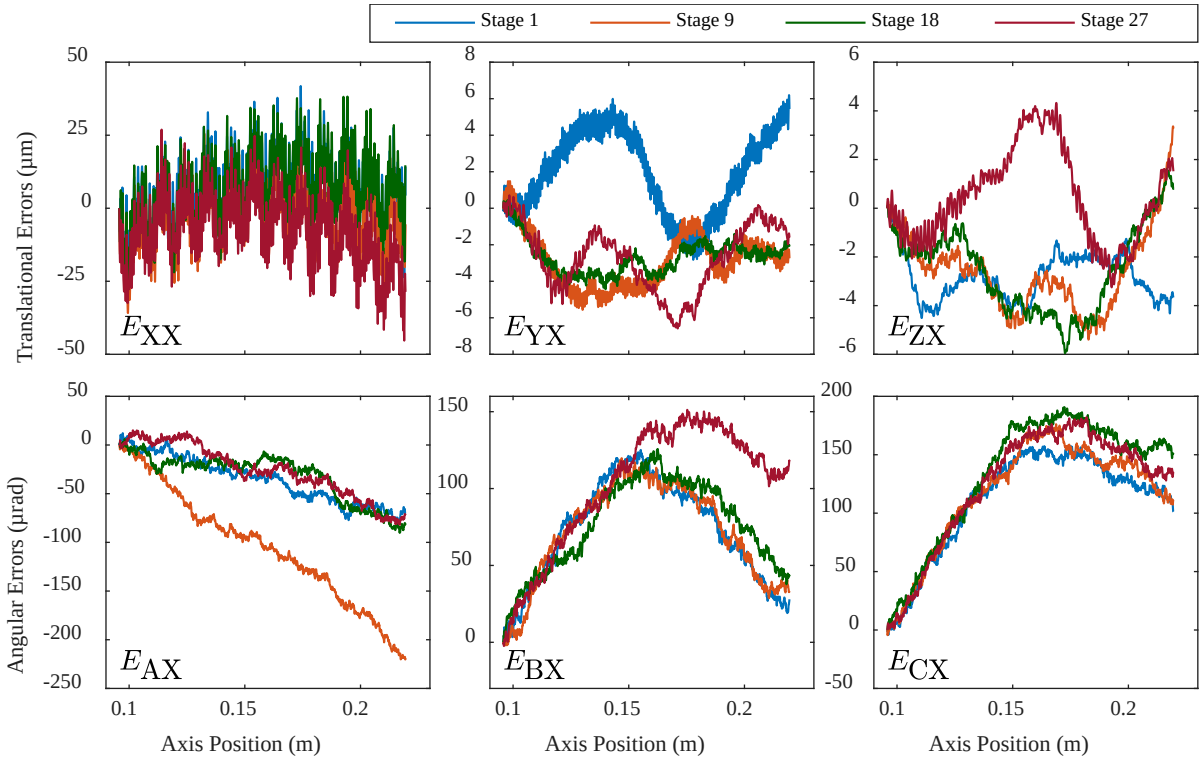

Figure 6: Unfiltered error motions of the carriage at four stages of bearing degradation. The error components are noted in the bottom left corner of each sub-figure.

Analysis Methods: The simplest analysis methods use only statistical and frequency domain features to analyze each instance of data. The statistical time-domain features used in the analysis of this experiment are given in Table 2, where $\bar{y}$ denotes the signal average and N denotes the number of data points in the signal. For the current implementation, each 'signal' of Table 2 is an error motion or some transformation of the sampled error motion, e.g., via filtering. Each of the values provided were computed for every instance of error motion data generated at the incrementally increasing stages of degradation.

Table 2: Description of statistical time-domain features used in bearing diagnostic analysis [12-15]

Feature name	**Brief description**	**Formula**
Peak value	The peak value measures the amplitude of the signal, y. As bearings faults develop, there are more impacts producing higher average amplitude, hence the peak value is expected to increase.	$PV(y) = \frac{1}{2}\left(\max(y) - \min(y)\right)$
RMS	The root mean square (RMS) of a signal is measure of the energy of the signal.	$rms(y) = \sqrt{\frac{1}{N}\sum_{i=1}^{N} y_i^2}$
Standard deviation	The standard deviation measures the dispersion of the signal around the mean value, which is another measure of the amplitude and energy in the signal.	$\sigma(y) = \sqrt{\frac{1}{N-1}\sum_{i=1}^{N}(y_i - \bar{y})^2}$
Skewness	Skewness quantifies the asymmetry of the signal with respect to its probability density function.	$\gamma_1(y) = \frac{\frac{1}{N}\sum_{i=1}^{N}(y_i - \bar{y})^3}{\sigma^3}$
Kurtosis	Kurtosis quantifies the "tailedness" of a signal. As a bearing degrades, more impacts are expected. This leads to a signal having more frequent and extreme deviations than a signal from a healthy bearing.	$\gamma_2(y) = \frac{\frac{1}{N}\sum_{i=1}^{N}(y_i - \bar{y})^4}{\sigma^4}$
Crest factor	Crest factor is a ratio of the peak value to the RMS. If there are impacts from a degraded bearing, then this value will be high, due to the discrepancy between the high peak produced from the impacts and the nominal amplitude of the waveform.	$CF(y) = \frac{PV(y)}{rms(y)}$
Shape factor	Shape factor is a ratio between the RMS and the average absolute value. Since RMS measures the square of the signal, then it will be more sensitive to outliers, such as impacts. So as bearings get more degraded, the shape factor is expected to increase.	$SF(y) = \frac{rms(y)}{\frac{1}{N}\sum_{i=1}^{N}\lvert y_i \rvert}$

Table 2: Description of statistical time-domain features used in bearing diagnostic analysis [12-15]

Feature name	Brief description	Formula
Impulse factor	As bearings degrade, they are expected to produce more impacts, which will greatly affect the peak value, but will have a smaller effect on the average absolute value. Hence, as bearings degrade, the impulse factor is expected to increase.	$IF(y) = \frac{PV(y)}{\frac{1}{N}\sum_{i=1}^{N}\lvert y_i\rvert}$
Clearance factor	The clearance factor is also a measure that relates the peak value to a measure of the average amplitude. As the bearings degrades and more impulses are produced, the numerator should rise while the denominator remains almost constant.	$CLF(y) = \frac{PV(y)}{\left(\frac{1}{N}\sum_{i=1}^{N}\sqrt{\lvert y_i\rvert}\right)^2}$

Beyond computing these statistical features from the error motions, many signal processing procedures have been proposed in the bearing community. Most of the proposed techniques aim to increase the kurtosis of the signal, in order to isolate changes due to impulses from degradation. These techniques include autoregressive (AR) filtering, self-adaptive noise cancellation (SANC), minimum entropy deconvolution (MED), and spectral kurtosis (SK). The AR filtering and SANC are both methods of separating the deterministic portion of the signal from the random portion of the signal [16]. In both cases, a prediction is computed, then the residual between the predicted signal and the real signal is considered as the bearing signal. In this study, only AR filtering was used.

The AR filter predicts the deterministic pattern of the signal, but is not capable of adapting to the sudden impulses caused by bearing faults. Consequently, the fault signal is expected to remain in the residual of the AR filter, which is the difference between the measured signal and the estimated signal (i.e., the output of the AR filter). An $AR(L)$ (i.e., an L^{th} order AR process) process is one in which the signal is assumed to be given as a linear combination of L past values and some input, e_n, as shown in (1):

$$x_n = -\sum_{l=1}^{L} a_l x_{n-l} + e_n \tag{1}$$

By assuming the input is unknown, the signal can be approximately predicted from the linear summation of past samples. This is computed as shown in (2).

$$\hat{x}_n = -\sum_{l=1}^{L} a_l x_{n-l} \tag{2}$$

The residual is then computed as $e_n = x_n - \hat{x}_n$. The model coefficients can be computed through a variety of methods, though perhaps the most used is the Yule-Walker equations, which relate the model coefficients to the autocovariance of the signal [16]. The order of the AR model (i.e., the number of model coefficients) can be chosen using a variety of criteria, such as Akaike information criteria (AIC), Bayesian information criteria (BIC), or cross validation. However, in the present study, the AR model order was chosen as the number of coefficients that maximized the kurtosis of the residual, in an attempt to isolate the defect-caused terms from the error motion data.

After separating out the bearing signal via AR (or SANC) filtering, the impulsive fault signal can be enhanced using MED, which was originally proposed by Wiggins [17] to extract information from seismic recordings. MED operates under the assumption that the original excitation was impulsive (with high kurtosis), then designs a filter that attempts to reconstruct the original signal. This is a means to overcome the effect of the transmission path through which the impulses reach the sensor(s). Since impulsive signals are highly structured (low entropy), the desired filter should minimize the signal entropy. Sawalhi *et al*. [18] applied MED to bearing faults, Endo and Randall [19] used it with gear faults, and Randall and Antoni [11] recommended its use as part of a "semi-automated bearing diagnostic procedure". Lee and Nandi [20] and McDonald *et al*. [21] have provided comprehensive methods for computing MED. The procedure used herein is shown below.

Step 1: Assume a centered impulse filter, $\boldsymbol{f} = [0 \quad \cdots \quad 0 \quad 1 \quad 0 \quad \cdots \quad 0]^T$, of length L

Step 2: Compute the $L \times L$ autocorrelation matrix $\boldsymbol{R}_x$; a Toeplitz matrix with the first row as the first L terms of the autocorrelation of $\boldsymbol{x}$

Step 3: Compute filter output, $\boldsymbol{y} = \boldsymbol{X}_0^T \boldsymbol{f}$

Step 4: Compute new filter: $\boldsymbol{f} = \frac{\sum_{i=1}^{N} y_i^2}{\sum_{i=1}^{N} y_i^4} \boldsymbol{R}_x^{-1} \boldsymbol{X}_0 \boldsymbol{y}^3$

Step 5: Repeat steps 3-4 until stopping criterion are satisfied

Here, $\boldsymbol{y}^3$ is an element-wise cubing of the filtered signal, and $\boldsymbol{X}_0$ is an $L \times N$ matrix of the delayed input signal:

$$\boldsymbol{X}_0 = \begin{bmatrix} x_1 & x_2 & x_3 & \cdots & x_N \\ 0 & x_1 & x_2 & \cdots & x_{N-1} \\ 0 & 0 & x_1 & \cdots & x_{N-2} \\ \vdots & \vdots & \vdots & \ddots & \vdots \\ 0 & 0 & 0 & \cdots & x_{N-L+1} \end{bmatrix}$$

The stopping criterion can be based upon the change in the filtered signal kurtosis (i.e., once the change in filtered signal kurtosis reaches a sufficiently small value) as proposed by McDonald *et al*. [21]. Or the stopping criterion can be based upon changes in the filter as proposed by Lee and Nandi [20], stating that when $E[\boldsymbol{\epsilon}]$ gets below a certain threshold, the routine is complete.

$$\boldsymbol{\epsilon} = \left(\boldsymbol{f}^{(i)} - \mu \boldsymbol{f}^{(i-1)}\right)/\mu \boldsymbol{f}^{(i-1)} \tag{3}$$

$$\mu = \sqrt{\frac{E[(\boldsymbol{f}^{(i-1)})^2]}{E[(\boldsymbol{f}^{(i)})^2]}}$$

In (3), the expressions are shown for the ith iteration, $\left(\boldsymbol{f}^{(i)}\right)^2$ is an element-wise squaring of the vector $\boldsymbol{f}^{(i)}$, and $E[\cdot]$ denotes the expected value. In this study, the criterion proposed by Lee and Nandi was used with the threshold for $E[\boldsymbol{\epsilon}]$ set to $5(10^{-4})$.

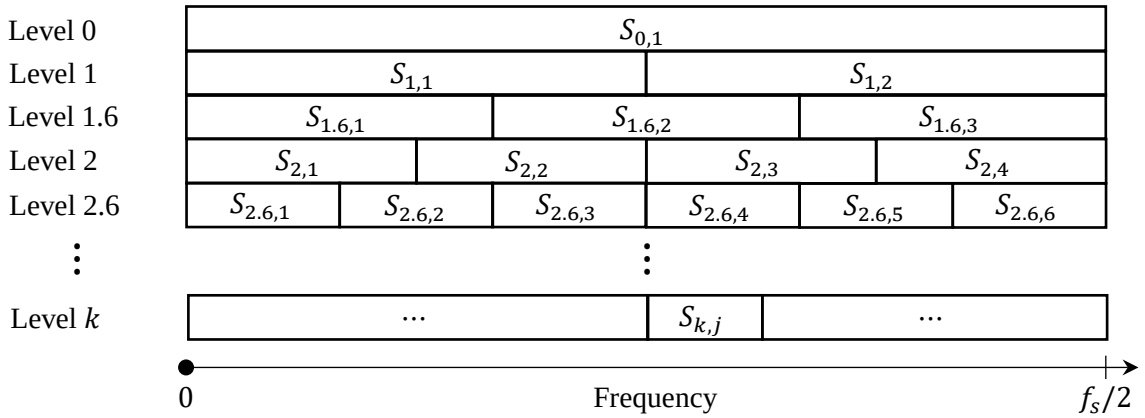

Figure 7: Frequency and decomposition levels for construction of kurtogram.

The last step in the process is to use spectral kurtosis and the kurtogram to locate the frequency band and frequency resolution that maximizes the signal kurtosis. The kurtogram is a method that uses a finite impulse response (FIR) filter bank to decompose the signal into a set of subsignals with different frequency bands [22]. This decomposition consists of taking the signal, then low-pass- and high-pass-filtering to the frequency bands $[0, 1/4]$ and $[1/4\,, 1/2]$, respectively (in normalized frequency). This is considered as Level 1 decomposition. The original signal is also decomposed into the frequency bands $[0, 1/6]$, $[1/6\,, 1/3]$, and $[1/3\,, 1/2]$. This is considered as Level 1.6 decomposition. Then the resulting signals are sent through further replicate filter banks, producing an arborous structure as shown in Figure 7, where $S_{k,j}$ represents the signal decomposed at level k in the jth frequency band, and f_s is the sampling frequency. After the signals are decomposed, the kurtosis of each $S_{k,j}$ can be computed, and the level and frequency band that maximizes kurtosis chosen.

Experimental Analysis Results: The error motions were first high-pass filtered to frequencies above 500 samples/m, which was done to eliminate any data that simply captured the shape of the rails. Bearing fault signatures are assumed to occur with wavelengths less than about 12.4 mm (circumference of a single ball), therefore sampling between 0.5 samples/mm and 2 samples/mm is sufficient to capture any impacts from bearing faults. Most of the statistical metrics yielded no indications of the increasing number of faults being introduced to the balls of truck 2. As an example, the kurtosis of each sample is shown in Figure 8. There are 27 total stages, and at each stage, there are 50 runs, translating to 50 values of kurtosis. At each stage,

the gray box represents the middle 50% of these 50 values, and the whiskers extend to the largest value that falls below $q_3 + 1.5(q_3 - q_2)$, or the smallest value that falls above $q_2 - 1.5(q_3 - q_2)$, where q_2 and q_3 are the 25th and 75th percentile respectively. Any value that falls outside this range is classified as an outlier, and the outliers are plotted as red circles. The black circle in the center of each box is the median value for all 50 runs in a given degradation stage.

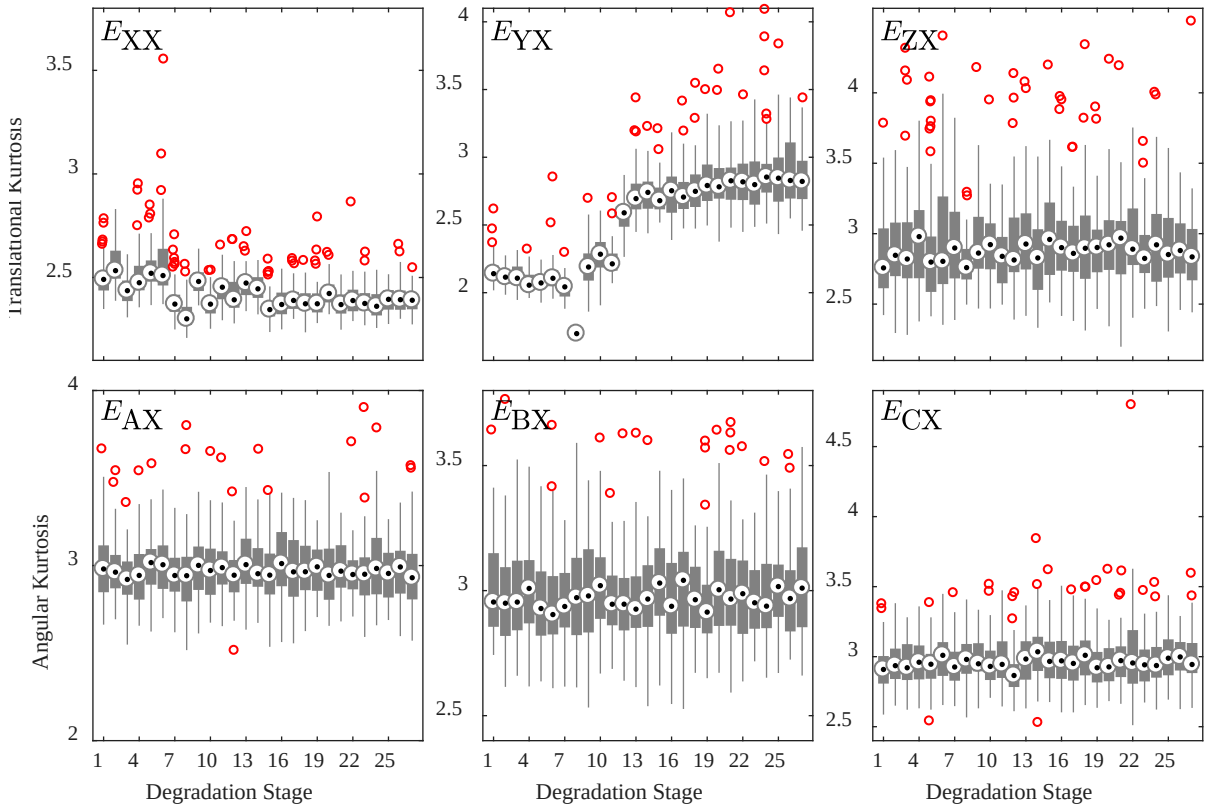

Figure 8: Boxplots showing how the filtered signal kurtosis changed as additional degradations were introduced into Truck 2 outer ring.

The statistical features can be evaluated using the Pearson correlation coefficient between the median of each distribution of 50 samples and the degradation stages (1-27). Because Pearson correlation measures the strength of a linear relationship between two variables, it is expected that as a feature is more responsive to bearing degradation, it will register a higher Pearson correlation coefficient magnitude. The sign of the Pearson correlation coefficient indicates the direction of the line, where $+1$ indicates the line is increasing and -1 indicates the line is decreasing. The Pearson correlation coefficient for each feature and DOF is shown in Figure 9.

From Figure 8 and Figure 9, it is apparent that E_{YX} trends the most as the bearings of Truck 2 outer loop are degraded, since most of its statistical features have Pearson correlation coefficients with magnitudes significantly above 0.5. Furthermore, E_{XX} has a moderate trend in kurtosis and E_{ZX} has a moderate trend in skewness, each with Pearson correlation coefficient magnitudes around 0.5. Moreover, in the case of E_{YX}, the kurtosis starts as lower than that of the normal distribution (which has a kurtosis of 3) and ends with most runs still below a

kurtosis of 3, but having a higher kurtosis than at Stage 1. Generally, when bearings are faulty, the impacts that the bearings have with the runways produce kurtosis values much higher than that of normal distribution (see e.g., [18, 23]). This physical trend should be further examined for further understanding. Also, it must be noted that the error motion data under examination are high-pass filtered and not unprocessed.

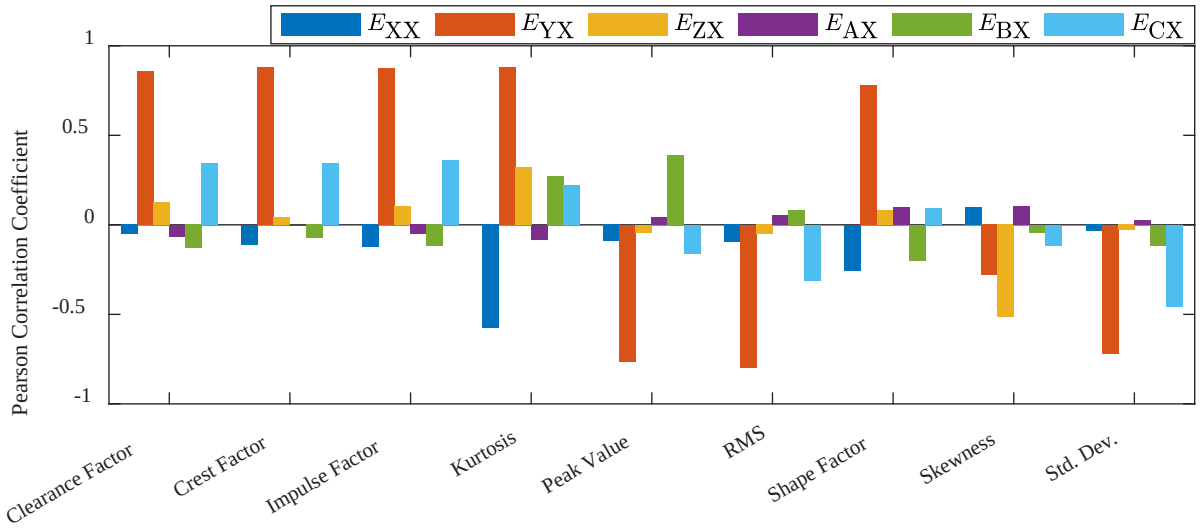

Figure 9: Pearson correlation coefficient for each statistical feature computed.

After performing the procedure recommended by Randall and Antoni, the results for one response are shown in Figure 10. The data was first high-pass-filtered to above 500 m^{-1}, then an $AR(26)$ filter was used to eliminate the deterministic portion of the signal. The length of the AR filter was found by exhaustively searching all error directions. Each signal was filtered using filter lengths between 2 and 400, and the kurtosis was measured for each filtered signal. For all error directions, the optimal length that maximized filtered signal kurtosis was between 25 and 28, with an average of 26. After AR filtering, the MED filter of length 10 was used. The length of the MED filter was also chosen according to the length that maximized signal kurtosis. Finally, the kurtogram was used on the MED filtered signal.

After processing all six DOF error motion data in the manner shown in Figure 10, the kurtosis values are shown using boxplots in Figure 11, à la Figure 8. In most cases, the kurtosis achieved using the MED filter was very close to the kurtosis achieved using the kurtogram. More importantly, like the simple statistical analysis results shown in Figure 8, the straightness errors in the Y-direction exhibit the most movement in Figure 11 as the ball bearings were degraded. Also, as shown in comparison of Figure 11 to Figure 8, this signal kurtosis was increased by decomposing the MED filtered signal to Level 1 with center frequency of $f_s/8 = 2500$ m^{-1}. However, it appears that the kurtogram may have decreased the robustness for monitoring changes in degradation, because the kurtogram increased the variance of the kurtosis of E_{YX}, as evidenced by the significantly longer gray boxes for E_{YX} in Figure 11 compared with those for E_{YX} in Figure 8.

These results show that certain metrics lack no significant trends with increasing degradation, which could result from several possibilities. First, the faulty bearings occurred in only one of

two bearing loops in one of four trucks on the linear axis, so it is possible that the degradation in one bearing ball loop does not significantly affect certain error motions due to the influence of seven healthy bearing ball loops and the geometry of the raceways. Second, the signal processing techniques used were designed for temporal measurements (i.e., vibration as a function of time) that typically have many cycles for each dataset due to the rotary nature of the applications (e.g., spindles and motors). On the other hand, each run collected by the IMU has on the order of only one cycle of ball motion, in which the balls move in and out of contact between the truck and rail. Furthermore, because of the approximately one cycle of ball motion and recirculation of balls, the spatial locations of the defect-caused impulses along the rail are constantly moving, sometimes to outside of the spatial measurement range. Third, the ceramic balls were nominally 7 µm larger in diameter than the metal balls, which means that as more metal balls were degraded, the ceramic balls were bearing more of the load, which could account for apparent approaching of relative equilibria in Figure 8.

Finally, the results raise many questions for future work:

1. What is the lowest amount of damage that can be detected with the IMU via the methods explored or any other?
2. Why is the Y-direction most sensitive to changes in the bearings?
3. What signal processing techniques could be used to increase the signal to noise ratio for earlier detection of degraded linear axis bearings?
4. How can signal processing techniques be adapted to dealing with spatial measurements, rather than temporal measurements?

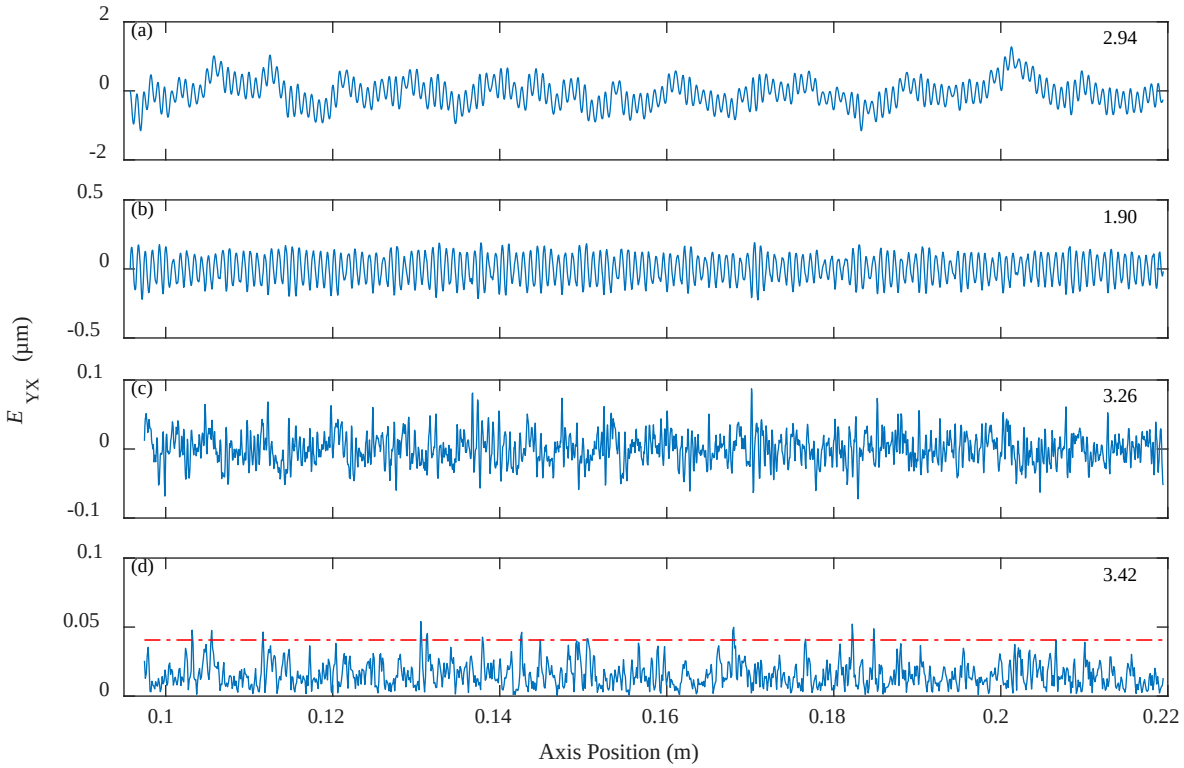

Figure 10: Semi-automated bearing diagnostic procedure for degradation stage 16, run 6, in y-axis translation, with the respective kurtosis values noted in the upper right corner of each

plot. (a) Error response filtered to spatial frequencies above 500 m^{-1}. (b) Residual of signal after $AR(26)$ filtering of the signal from (a). (c) Signal after MED (filter length of 10) of signal from (b). (d) Magnitude of complex envelope of the signal from (c) which maximized the kurtogram (level 1 decomposition) and its 0.1% significance threshold (shown in red).

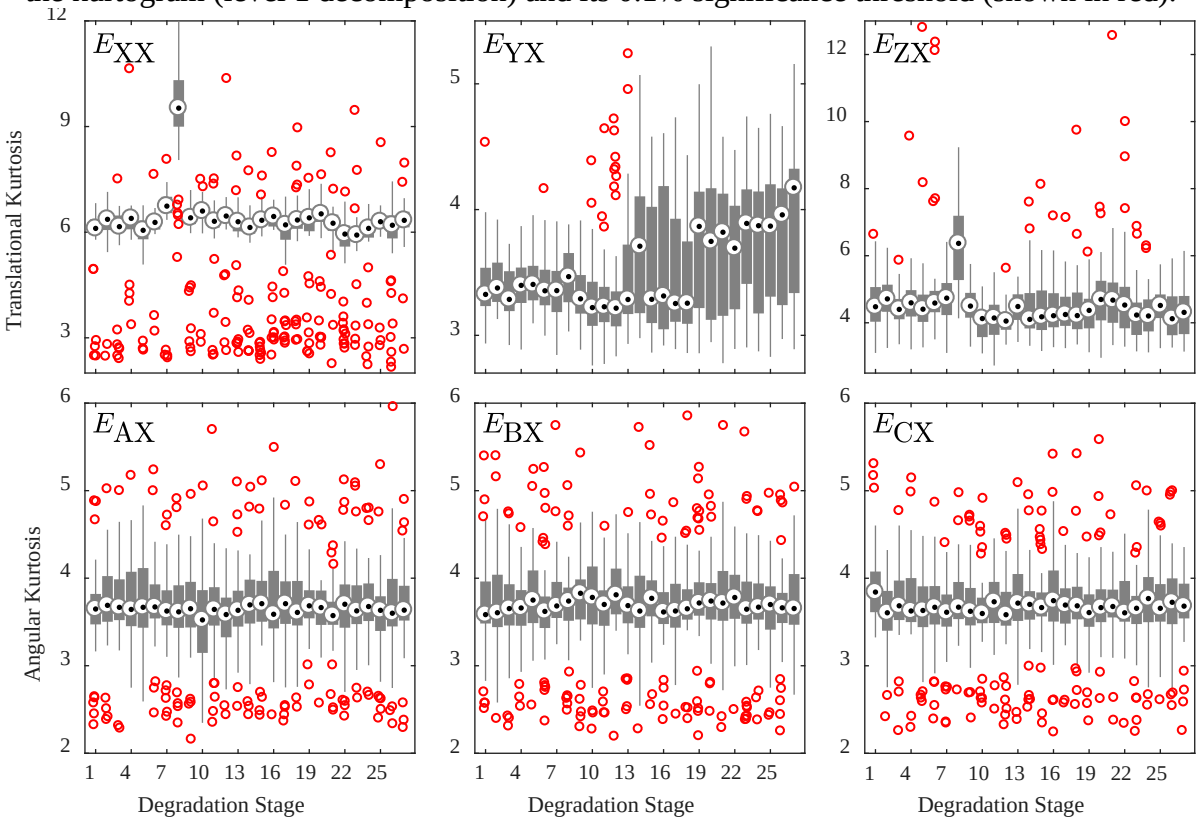

Figure 11: Kurtosis values resulting from the bearing diagnostics procedure.

Conclusion: The linear axis is used in a variety of machining processes and their bearings are subject to wear. This paper presented an experiment wherein an inertial measurement unit (IMU) was employed to detect degraded bearings in a linear axis. The six DOF error motions for the carriage were first analyzed for statistical features and then signal processing techniques were used to amplify the signal of degraded bearings. The results showed the error motions, determined from processing IMU data, experienced some evolution over time, particularly in the Y-direction (error motion described as E_{YX}). Pearson correlation coefficients showed additional trends detected by kurtosis for the translation in the X-direction (E_{XX}) and skewness for translation in the Z-direction (E_{ZX}). However, certain metrics lacked no significant trends with increasing degradation, which could have resulted from the experimental setup (lack of cycles per run), physical phenomena (effects of degradation, recirculation of balls), and the analytical techniques themselves. The results motivate further research into fault detection and diagnostics for linear axes, with an emphasis on identifying the optimal techniques suited to the unique problem of linear translation.

NIST Disclaimer: Certain commercial equipment, instruments, or materials are identified in this paper to foster understanding. Such identification does not imply recommendation or

endorsement by the National Institute of Standards and Technology, nor does it imply that the materials or equipment identified are necessarily the best available for the purpose.

References:

[1] Y. Altintas, A. Verl, C. Brecher, L. Uriarte, and G. Pritschow, "Machine tool feed drives," *CIRP Annals - Manufacturing Technology,* vol. 60, no. 2, pp. 779-796, // 2011.

[2] Y. Li, X. Wang, J. Lin, and S. Shi, "A Wavelet Bicoherence-Based Quadratic Nonlinearity Feature for Translational Axis Condition Monitoring," *Sensors,* vol. 14, no. 2, pp. 2071-2088, 2014.

[3] Y. Zhou, X. Mei, Y. Zhang, G. Jiang, and N. Sun, "Current-based feed axis condition monitoring and fault diagnosis," in *4th IEEE Conference on Industrial Electronics and Applications, ICIEA 2009*, Xi'an, China, 2009, pp. 1191-1195: IEEE Computer Society.

[4] E. Uhlmann, C. Geisert, and E. Hohwieler, "Monitoring of slowly progressing deterioration of computer numerical control machine axes," *Proceedings of the Institution of Mechanical Engineers, Part B: Journal of Engineering Manufacture,* vol. 222, no. 10, pp. 1213-1219, 2008.

[5] *ISO 230-1 - Test code for machine tools − Part 1: Geometric accuracy of machines operating under no-load or quasi-static conditions*, 2012.

[6] A. W. Khan and W. Chen, "Calibration of CNC milling machine by direct method," in *2008 International Conference on Optical Instruments and Technology: Optoelectronic Measurement Technology and Applications*, Beijing, China, 2009, vol. 7160, p. 716010: SPIE.

[7] R. Teti, K. Jemielniak, G. O'Donnell, and D. Dornfeld, "Advanced monitoring of machining operations," *CIRP Annals - Manufacturing Technology,* vol. 59, no. 2, pp. 717-739, 2010.

[8] G. W. Vogl, M. A. Donmez, and A. Archenti, "Diagnostics for geometric performance of machine tool linear axes," *CIRP Annals - Manufacturing Technology,* vol. 65, no. 1, pp. 377-380, 2016.

[9] G. W. Vogl, M. A. Donmez, A. Archenti, and B. A. Weiss, "Inertial Measurement Unit for On-Machine Diagnostics of Machine Tool Linear Axes," presented at the Annual Conference of the Prognostics and Health Management Society 2016, Denver, CO, October 3 - 6, 2016, 2016.

[10] G. W. Vogl and M. E. Sharp, "Diagnostics of machine tool linear axes via separation of geometric error sources," presented at the Annual Conference of the Prognostics and Health Management Society, St. Petersburg, FL, October 2-5, 2017, 2017.

[11] R. B. Randall and J. Antoni, "Rolling element bearing diagnostics—A tutorial," *Mechanical systems and signal processing,* vol. 25, no. 2, pp. 485-520, 2011.

[12] W. Caesarendra and T. Tjahjowidodo, "A review of feature extraction methods in vibration-based condition monitoring and its application for degradation trend estimation of low-speed slew bearing," *Machines,* vol. 5, no. 4, p. 21, 2017.

[13] I. Howard, "A Review of Rolling Element Bearing Vibration'Detection, Diagnosis and Prognosis'," Defence Science and Technology Organization Canberra (Australia)1994.

[14] B. Sreejith, A. Verma, and A. Srividya, "Fault diagnosis of rolling element bearing using time-domain features and neural networks," in *Industrial and Information Systems, 2008. ICIIS 2008. IEEE Region 10 and the Third international Conference on*, 2008, pp. 1-6: IEEE.

[15] C. T. Yiakopoulos, K. C. Gryllias, and I. A. Antoniadis, "Rolling element bearing fault detection in industrial environments based on a K-means clustering approach," *Expert Systems with Applications*, vol. 38, no. 3, pp. 2888-2911, 2011/03/01/ 2011.

[16] R. Randall, N. Sawalhi, and M. Coats, "A comparison of methods for separation of deterministic and random signals," *International Journal of Condition Monitoring*, vol. 1, no. 1, pp. 11-19, 2011.

[17] R. A. Wiggins, "Minimum entropy deconvolution," *Geoexploration*, vol. 16, no. 1, pp. 21-35, 1978/04/01/ 1978.

[18] N. Sawalhi, R. B. Randall, and H. Endo, "The enhancement of fault detection and diagnosis in rolling element bearings using minimum entropy deconvolution combined with spectral kurtosis," *Mechanical Systems and Signal Processing*, vol. 21, no. 6, pp. 2616-2633, 2007.

[19] H. Endo and R. B. Randall, "Enhancement of autoregressive model based gear tooth fault detection technique by the use of minimum entropy deconvolution filter," *Mechanical Systems and Signal Processing*, vol. 21, no. 2, pp. 906-919, 2007.

[20] J.-Y. Lee and A. Nandi, "Extraction of impacting signals using blind deconvolution," *Journal of Sound and Vibration*, vol. 232, no. 5, pp. 945-962, 2000.

[21] G. L. McDonald, Q. Zhao, and M. J. Zuo, "Maximum correlated Kurtosis deconvolution and application on gear tooth chip fault detection," *Mechanical Systems and Signal Processing*, vol. 33, pp. 237-255, 2012.

[22] J. Antoni, "Fast computation of the kurtogram for the detection of transient faults," *Mechanical Systems and Signal Processing*, vol. 21, no. 1, pp. 108-124, 2007/01/01/ 2007.

[23] J. Antoni and R. Randall, "The spectral kurtosis: application to the vibratory surveillance and diagnostics of rotating machines," *Mechanical Systems and Signal Processing*, vol. 20, no. 2, pp. 308-331, 2006.